A Decanuclear Manganese Cluster with Oxo and Halide Bridging Ligands: Magnetic Behavior of an $S \geq 12$ System

David P. Goldberg,[†] Andrea Caneschi,[‡] Christopher D. Delfs,[‡] Roberta Sessoli,*[,‡] and Stephen J. Lippard*[,†]

Contribution from the Department of Chemistry, Massachusetts Institute of Technology, Cambridge, Massachusetts 02139, and Dipartimento di Chimica, Universita' degli Studi di Firenze, Italia 50144

Received December 22, 1994[⊗]

Abstract: The reaction of 2,2′-biphenoxide with simple manganese halide salts affords novel mixed-valent decanuclear complexes of formula $[Mn_{10}O_4(biphen)_4X_{12}]^{4-}$ ($X = Cl^-$, Br^-). The syntheses of three related compounds in this class, $[Me_4N]_4[Mn_{10}O_4(biphen)_4Cl_{12}]$ (**1**), $[Me_4N]_4[Mn_{10}O_4(biphen)_4Br_{12}]$ (**2**), and $[Mn(CH_3CN)_4(H_2O)_2][Et_3NH]_2[Mn_{10}O_4(biphen)_4Br_{12}]$ (**3**), are described. These complexes have been structurally characterized by X-ray diffraction, details of which are reported for **2**. Compounds **1**–**3** belong to a very small class of high-nuclearity manganese clusters held together by bridging ligands other than the carboxylate moiety. They are mixed-valent, with four Mn(III) atoms and six Mn(II) atoms comprising the cluster. All of the manganese centers are valence-localized, the octahedral Mn(III) sites being delineated by marked Jahn–Teller axial elongations. The bridging ligands bind in a variety of modes, there being four μ_4-oxo ligands at the core of the cluster. The magnetic properties of compounds **1**–**3** were investigated in the polycrystalline state by magnetic susceptibility and high-field magnetization measurements, which revealed high-spin ground states ($12 \leq S \leq 14$). The χT curve for **2** steadily increased from 37.9 emu mol^{-1} K at 300 K to 95.1 emu mol^{-1} K at 5 K. The high-field magnetization curve reached a plateau at a value of 28.3 μ_B for the reduced magnetization. Single-crystal susceptibility and X-band cw-EPR measurements on **3** showed an Ising-type anisotropy in the magnetization for this compound, with $\chi_{\parallel}T = 128$ emu mol^{-1} K at 2.2 K, and $\chi_{\perp}T = 46$ emu mol^{-1} K at 2.1 K. The magnitude of the overall zero-field splitting parameter, D, for the $S = 12$ ground state was calculated to be $|D| = |0.035|$ cm^{-1} from the single crystal EPR data. Theoretical calculations based on simplified models are presented which provide a framework in which to understand the origin of the high-spin ground states for these complexes.

Introduction

The synthesis and magnetic properties of high-nuclearity (≥4) manganese compounds have been the focus of intense research efforts in recent years. The large majority of these compounds are composed of manganese atoms in the +2, +3, or +4 oxidation states, with carboxylato and oxo ligands forming the bridges between metal centers. Impetus for studying the structural and physical properties of this class of molecules has come from a variety of sources including the need for bioinorganic models of the polynuclear manganese core in Photosystem II,[1] interest in polynuclear compounds of iron and manganese as possible molecular units for the construction of magnetic materials,[2] and the potential of high-nuclearity spin clusters to provide examples of structurally characterized nanometer-scale materials in which each cluster can be considered as an independent single-domain particle.[3,4] Large clusters of this kind have the ideal mesoscopic dimensions to observe the coexistence of classical and quantum magnetization behavior. They also represent a new phase of magnetism that lies between the simple paramagnetism of isolated molecules and the bulk magnetism of extended lattices. The possibility of observing magnetic hysteresis at the molecular level opens new perspectives in the field of molecular memory.

With the above areas of interest in mind, we and others have synthesized a variety of polynuclear iron and manganese complexes and characterized them crystallographically and by several other physical techniques. Mn_4 compounds have been prepared which exhibit either a "butterfly"[5,6] or "distorted cubane"[7–10] structural motif and which form the basic unit of many of the higher nuclearity assemblies. Discrete complexes containing more than four atoms are considerably fewer in number. Examples include three Mn_6 compounds, one of which has six Mn(II) ions arranged in a ring and bridged by nitronyl nitroxide ligands,[11] whereas the other two comprise smaller Mn_4O_2 butterfly-type units.[12–15] An Mn_7 compound has been described having six Mn(III) atoms and one Mn(II) atom,

[†] Massachusetts Institute of Technology.

[‡] Universita' degli Studi di Firenze.

[⊗] Abstract published in *Advance ACS Abstracts*, May 1, 1995.

(1) Debus, R. J. *Biochim. Biophys. Acta* **1992**, *1102*, 269–352.

(2) McCusker, J. K.; Schmitt, E. A.; Hendrickson, D. N. In *Magnetic Molecular Materials*; Gatteschi, D., Kahn, O., Miller, J. S., Palacio, F., Eds.; Kluwer Academic Publishers: Dordrecht, The Netherlands, 1991; pp 297–319.

(3) Caneschi, A.; Gatteschi, D.; Pardi, L.; Sessoli, R. *Science* **1994**, *265*, 1054.

(4) Papaefthymiou, G. *Phys. Rev. B* **1992**, *46*, 10366–10375.

(5) Vincent, J. B.; Christmas, C.; Huffman, J. C.; Christou, G.; Chang, H.-R.; Hendrickson, D. N. *J. Chem. Soc., Chem. Commun.* **1987**, 236–238.

(6) Christou, G. *Acc. Chem. Res.* **1989**, *22*, 328–335.

(7) Wang, S.; Folting, K.; Streib, W. E.; Schmitt, E. A.; McCusker, J. K.; Hendrickson, D. N.; Christou, G. *Angew. Chem., Int. Ed. Engl.* **1991**, *30*, 305–306.

(8) Wang, S.; Tsai, H.-L.; Streib, W. E.; Christou, G.; Hendrickson, D. N. *J. Chem. Soc., Chem. Commun.* **1992**, 1427–1429.

(9) Hendrickson, D. N.; Christou, G.; Schmitt, E. A.; Libby, E.; Bashkin, J. S.; Wang, S.; Tsai, H.-L.; Vincent, J. B.; Boyd, P. D. W.; Huffman, J. C.; Folting, K.; Li, Q.; Streib, W. *J. Am. Chem. Soc.* **1992**, *114*, 2455–2471.

(10) Wemple, M. W.; Tsai, H.-L.; Folting, K.; Hendrickson, D. N.; Christou, G. *Inorg. Chem.* **1993**, *32*, 2025–2031.

(11) Caneschi, A.; Gatteschi, D.; Laugier, J.; Rey, P.; Sessoli, R.; Zanchini, C. *J. Am. Chem. Soc.* **1988**, *110*, 2795–2799.

(12) Baikie, A. R. E.; Howes, A. J.; Hursthouse, M. B.; Quick, A. B.; Thornton, P. *J. Chem. Soc., Chem. Commun.* **1986**, 1587.

0002-7863/95/1517-5789$09.00/0

arranged as two butterfly-type units sharing one wing-tip metal atom,[16] and a similar Mn_7 compound with all Mn(III) atoms has been reported.[17] The preparation of three types of Mn_8 compounds has been accomplished by using Mn_4 butterfly-type compounds as starting materials, and these octanuclear complexes reveal structures consistent with a shared motif of this kind.[18-21] The two structural types of Mn_9 compounds reported thus far are each also composed of smaller, butterfly-type Mn_4O_2 units. One type is mixed-valent with eight Mn(III) atoms and one central Mn(II) atom linking two butterfly units through salicylate bridging ligands,[22] whereas the other type has nine Mn atoms in the +3 oxidation state with oxo, carboxylato bridges and either pyridine ligands[23] or an $[Na_2(O_2CPh)_2(MeCN)_2]$ unit occupying external coordination sites.[19]

The two known Mn_{10} complexes, in addition to the one described here, are distinguished by their novel architecture, which does not contain Mn_4O_2 butterfly-type units; they are assembled in the absence of carboxylate ligands. One of these molecules, $[Mn_{10}O_{14}(tren)_6](CF_3SO_3)_8$, tren = $N(CH_2CH_2NH_2)_3$, is a $Mn(III)_4Mn(IV)_6$ compound with a layered structure resembling the manganese oxide minerals chalcophanite and lithiophorite.[24] Another Mn_{10} compound, $(Et_4N)_2[Mn_{10}O_2Cl_8\{(OCH_2)_3CMe\}_6]$, is an $Mn(III)_8Mn(II)_2$ complex held together by multiply-bridging oxo groups and six tris(alkoxy) donor ligands.[25]

A single undecanuclear complex of composition $[Mn_{11}O_{10}Cl_2(OAc)_{11}(bpy)_2(MeCN)_2(H_2O)_2](ClO_4)_2 \cdot 8MeCN$ has been prepared and crystallographically characterized. The mixed-valent cluster in this complex has two $\{Mn(III)_3Mn(IV)O_3Cl\}^{6+}$ distorted cubane subunits linked by a central linear $\{Mn(III)_3O_4\}^{+}$ unit. The cubane substructures are similar to species mentioned above, but the linear Mn_3 unit has not been observed in a discrete ion. This compound was prepared by addition of the carboxylate-abstracting agent Me_3SiCl to an Mn_4 butterfly-type starting material, a procedure employed with great success for the preparation of higher nuclearity compounds.[26]

A dodecanuclear manganese complex, containing eight metal atoms in the +3 oxidation state and four in the +4 state, was first reported by Lis.[27] This cluster exhibited spectacular magnetic properties, including a high-spin $S = 10$ ground state[28] and a highly anisotropic magnetization, as well as a remarkably long magnetization relaxation time which gave rise to a pronounced magnetic hysteresis effect.[29] Recently a reduced form of this complex has been prepared, containing four Mn(IV) and seven Mn(III) atoms and one Mn(II) atom.[30] The Mn_6 nitronyl nitroxide compound[11] discussed above is the only other discrete molecule, beside the Mn_{10} cluster described here, which exhibits a spin multiplicity exceeding $S = 10$. A hexadecamanganese aggregate of formula $[Mn_{16}Ba_8Na_2ClO_4(OH)_4(CO_3)_4(H_2O)_{22}L_8]$, where L = 1,3-diamino-2-hydroxypropane-*N*,*N*,*N'*,*N'*-tetraacetic acid, has also been crystallographically characterized. This compound has the highest nuclearity known for a discrete polymanganese complex, but the magnetic properties have as yet not been described.[31]

Previously we communicated the synthesis, structure, and magnetic properties of $[Me_4N]_4[Mn_{10}O_4(biphen)_4Cl_{12}]$ (**1**).[32] In the present article we report a significant extension of this work, including the preparation of two new bromide analogues, $[Me_4N]_4[Mn_{10}O_4(biphen)_4Br_{12}]$ (**2**) and $[Et_3NH]_2[Mn(CH_3CN)_4(H_2O)_2][Mn_{10}O_4(biphen)_4Br_{12}]$ (**3**). A comprehensive description of the magnetic behavior and high-spin ground states of these clusters is provided through single-crystal magnetic susceptibility, magnetization, and EPR measurements on **3**, as well as by powder susceptibility and high-field magnetization measurements on **2**. Values of $12 \leq S \leq 14$ for the ground states of compounds **1**-**3** are indicated by all of the magnetic data. The single-crystal EPR data provide a direct experimental measure of the overall axial zero-field splitting parameter, D, for the $S = 12$ ground state of compound **3**. A satisfactory theoretical simulation of the magnetization data was made by using the two empirically determined values for S and D. A theoretical treatment of the magnetic properties of these molecules is presented through a series of three models of increasing complexity. These models successfully explain the high-spin ground states of **1**-**3** in terms of the magnetic exchange coupling between the 10 metal spin sites and are fully consistent with all of the magnetic data.

Experimental Section

General Methods. All materials were obtained from commercial sources and used as received. Where indicated, manipulations and reactions were carried out under an inert atmosphere in a Vacuum Atmospheres drybox. FTIR spectra were obtained by using a Bio-Rad SPC3200 FTIR instrument.

$[Me_4N]_4[(Mn_{10}O_4(biphen)_4X_{12}]$ (X = Cl (1); X = Br (2)). To a solution of $MnCl_2 \cdot 4H_2O$ (0.40 g, 2.0 mmol) and biphenH_2 (0.90 g, 4.8 mmol) in EtOH (10 mL) was added $Me_4NOH \cdot 4H_2O$ (0.09 g, 0.50 mmol) to give a dark red-brown solution. The reaction mixture was stirred for 15 min and filtered to remove a brown precipitate. Layering or slow vapor diffusion of CH_2Cl_2 into the filtrate gave **1**$\cdot CH_2Cl_2$ as a dark red-brown crystalline solid. This material was isolated by filtration and air-dried, affording 0.060 g (14%) of product. The same procedure was followed empolying $MnBr_2 \cdot 4H_2O$ to give 0.080 g (15%) of **2** as a dark red-brown crystalline solid. Anal. Calcd for **1**$\cdot CH_2Cl_2$, $Mn_{10}C_{65}H_{82}Cl_{14}N_4O_{12}$ (M_r 2157.13): C, 36.19; H, 3.83; N, 2.60. Found: C, 35.95; H, 3.80; N, 2.54. Upon heating of **1** at 111 °C under vacuum for 24 h, the lattice solvent was removed. Anal. Calcd for **1**, $Mn_{10}C_{64}H_{80}$-

(13) Schake, A. R.; Vincent, J. B.; Li, Q.; Boyd, P. D. W.; Folting, K.; Huffman, J. C.; Hendrickson, D. N.; Christou, G. *Inorg. Chem.* **1989**, *28*, 1915-1923.
(14) Bhula, R.; Collier, S.; Robinson, W. T.; Weatherburn, D. C. *Inorg. Chem.* **1990**, *29*, 4027-4032.
(15) Blackman, A. G.; Huffman, J. C.; Lobkovsky, E. B.; Christou, G. *Polyhedron* **1992**, *11*, 251-255.
(16) Bhula, R.; Weatherburn, D. C. *Angew. Chem., Int. Ed. Engl.* **1991**, *30*, 688-689.
(17) Wang, S.; Tsai, H.-L.; Streib, W. E.; Christou, G.; Hendrickson, D. N. *J. Chem. Soc., Chem. Commun.* **1992**, 677-679.
(18) Libby, E.; Folting, K.; Huffman, J. C.; Christou, G. *J. Am. Chem. Soc.* **1990**, *112*, 5354-5356.
(19) Wang, S.; Huffman, J. C.; Folting, K.; Streib, W. E.; Lobkovsky, E. B.; Christou, G. *Angew. Chem., Int. Ed. Engl.* **1991**, *30*, 1672-1674.
(20) Libby, E.; Folting, K.; Huffman, C. J.; Huffman, J. C.; Christou, G. *Inorg. Chem.* **1993**, *32*, 2549-2556.
(21) Wemple, M. W.; Tsai, H.-L.; Streib, W. E.; Hendrickson, D. N.; Christou, G. *J. Chem. Soc., Chem. Commun.* **1994**, 1031-1033.
(22) Christmas, C.; Vincent, J. B.; Chang, H.-R.; Huffman, J. C.; Christou, G.; Hendrickson, D. N. *J. Am. Chem. Soc.* **1988**, *110*, 823-830.
(23) Low, D. W.; Eichhorn, D. M.; Draganescu, A.; Armstrong, W. H. *Inorg. Chem.* **1991**, *30*, 878-880.
(24) Hagen, K. S.; Armstrong, W.; Olmstead, M. M. *J. Am. Chem. Soc.* **1989**, *111*, 774-775.
(25) Cavaluzzo, M.; Chen, Q.; Zubieta, J. *J. Chem. Soc., Chem. Commun.* **1993**, 131-133.
(26) Perlepes, S. P.; Huffman, J. C.; Christou, G. *J. Chem. Soc., Chem. Commun.* **1991**, 1657-1659.
(27) Lis, T. *Acta Crystallogr.* **1980**, *B36*, 2042-2046.
(28) Sessoli, R.; Tsai, H.-L.; Schake, A. R.; Wang, S.; Vincent, J. B.; Folting, K.; Gatteschi, D.; Christou, G.; Hendrickson, D. N. *J. Am. Chem. Soc.* **1993**, *115*, 1804-1816.
(29) Sessoli, R.; Gatteschi, D.; Caneschi, A.; Novak, M. A. *Nature* **1993**, *365*, 141-143.
(30) Tsai, H.-L.; Eppley, H. J.; deVries, N.; Folting, K.; Christou, G.; Hendrickson, D. N. *J. Chem. Soc., Chem. Commun.* **1994**, 1745-1746.
(31) Gorun, S. M.; Stibrany, R. T. U.S. Patent 5,041,575, 1991.
(32) Goldberg, D. P.; Caneschi, A.; Lippard, S. J. *J. Am. Chem. Soc.* **1993**, *115*, 9299-9300.

Table 1. Crystallographic Data for Compound **2**·4CH_3CN·0.5·H_2O.

chemical formula	$Mn_{10}C_{72}H_{93}N_8Br_{12}O_{12.5}$
formula weight	2778.8
space group	$P2_1/n$
a (Å)	22.073(4)
b (Å)	17.903(3)
c (Å)	26.269(6)
β (deg)	117.17(1)
V (Å^3)	9680(3)
Z	4
ϱ_{calcd}, (g cm^{-3})	1.91
μ (cm^{-1})	62.8
range of 2θ (deg)	3−49
octants collected	$+h+k\pm l$
trans coeff	0.913−1.000
no. of unique data	16 682
data with $F_o^2 > 3\sigma(F_o^2)$	5674
R_{merge} (%)	8.9
no. of variables	632
$R(F_o)^a$	0.072
$R_w(F_o)^b$	0.064
goodness of fit	1.36
λ (Å)	0.710 69
T (°C)	−60

^{a} $R = \sum||F_o| - |F_c||/\sum|F_o|$. ^{b} $R_w = [(\sum w(|F_o| - |F_c|/\sum w|F_o|^2]^{1/2}$. $w = 1/\sigma^2(F_o)$.

$Cl_{12}N_4O_{12}$ (M_r 2072.17): C, 37.10; H, 3.89; N, 2.70. Found: C, 36.86; H, 3.85; N, 2.57. FTIR (KBr pellet): 1497, 1477, 1433, 1294, 1271, 1252, 1217, 1158, 1123, 1100, 1049, 1006, 948, 859, 837, 767, 729, 713, 669, 640, 611, 591, 540, 429 cm^{-1}. Anal. Calcd for **2**, $Mn_{10}C_{64}H_{80}Br_{12}N_4O_{12}$ (M_r 2605.59): C, 29.50; H, 3.09; N, 2.15. Found: C, 29.21; H, 2.95; N, 1.99.

$[Et_3NH]_2[Mn(CH_3CN)_4(H_2O)_2][Mn_{10}O_4(biphen)_4Br_{12}]$·6$CH_3CN$·2.5$H_2O$·$C_6H_6$ (3·6CH_3CN·2.5H_2O·C_6H_6). To a solution of $MnBr_2$·4H_2O (1.1 g, 3.83 mmol) and biphenH_2 (2.2 g, 11.8 mmol) in CH_3CN (90 mL) was added Et_3N (0.25 mL, 1.79 mmol) to give a dark red-brown solution. The reaction mixture was stirred for 15 min and filtered. Vapor diffusion of C_6H_6 into the CH_3CN reaction filtrate gave **3** as tetragonally-shaped dark red-brown crystals. Due to the slow air decomposition of crystals of **3** upon filtration and standing in air, the mother liquor containing crystals of **3** was degassed and brought into a glovebox. The crystals were isolated by decanting the mother liquor, washed with pentane (5 × 10 mL), and dried under vacuum for 10 min, to give 0.435 g (36%) of **3** as a crystalline solid. The presence of benzene was confirmed by the ^{1}H NMR spectrum of **3** in DMSO-d_6. Crystals of **3** were washed extensively with pentane and dried briefly in vacuum prior to the NMR measurement. The assignment of the benzene peak (δ 7.24) was corroborated by the increase in intensity of this peak with the addition of benzene to the NMR tube. Anal. Calcd for $Mn_{11}C_{86}H_{109}Br_{12}N_{12}O_{16.5}$ (M_r 3138.06): C, 32.92; H, 3.50; N, 5.36. Found: C, 33.45; H, 2.97; N, 5.02.

Crystallography. A dark red-brown crystal (0.25 × 0.26 × 0.40 mm) of **2**·4CH_3CN·0.5H_2O grown from CH_3CN/toluene was selected for study. X-ray data were collected with an Enraf-Nonius CAD-4F κ geometry diffractometer and graphite-monochromatized Mo K$\bar{a}$ radiation (λ = 0.710 69 Å). The crystal temperature (see Table 1) was maintained by the use of an Enraf-Nonius FR558-S liquid nitrogen cryostat. The crystal specimen was mounted on the end of a quartz fiber with silicone grease. The unit cell dimensions were obtained from a least-squares fit of 21 reflections with $2\theta \geq 24°$ and revealed the Laue symmetry to be $2/m$. The Laue symmetry was determined by the unit cell parameters and confirmed by the examination of axial photographs. Two computer programs, TRANS and TRACER,[33] were employed to provide further confirmation of the Laue symmetry. The crystal was determined to be of sufficient quality for data collection as judged by the examination of axial photographs, the quality of the unit cell, and the measurement of selected peak widths at half-height ($\Delta\bar{w}_{1/2}$) by open-counter ω scans.

Intensity data were collected with the $\omega-2\theta$ scan technique. The intensities of three standard reflections were measured after every 3600 s of exposure time. The data were corrected for Lorentz and polarization effects and corrected for absorption following the measurement of Ψ scans.[34] No decay correction was necessary since there was no significant fluctuation in the intensities of the three standard reflections. The direct methods program SIR-92[35] was used for the initial structure solution, and a final model was obtained by least-squares refinement in combination with difference Fourier syntheses.

The Mn, Br, and O atoms were refined by using anisotropic thermal parameters, and the C and N atoms were refined with isotropic thermal parameters. All of the cation and solvent molecules were well behaved except for one disordered Me_4N^+ cation. Several attempts at modeling its disorder, including the introduction of two cations at half-occupancy and the use of rigid groups, failed to afford a satisfactory refinement. The model of the disordered cation used in the final analysis was composed of one Me_4N^+ molecule at full occupancy, represented by N(8), C(76), C(77), C(78), and C(79). A peak of significant electron density was consistently found near this cation but not within bonding distance. This peak was successfully modeled by a water molecule at a half-occupancy, represented by O(13). The largest positive peak in the final difference Fourier map had an electron density of 1.44 e/Å^3 and was located in the region near C77.

Hydrogen atoms were placed at calculated positions (C−H = 0.95 Å), and their B values were fixed at 1.2 times the B_{eq} of the atom to which they were bound, unless otherwise indicated. They were included, but not refined, in the final least-squares cycles. Scattering factors for the non-hydrogen[36] and hydrogen atoms[37] and anomalous dispersion terms[38,39] were taken from their usual sources. All calculations were performed with a VAXstation 4000-90 computer and the teXsan software package.[40]

A summary of crystallographic data for **2** can be found in Table 1. Selected bond distances and angles for **2** are listed in Table 2. A complete listing of intramolecular bond distances, angles, atomic coordinates and B_{eq}, and anisotropic thermal parameters are given in supplementary Tables S1−S4.

Magnetic Susceptibility Studies. DC magnetic susceptibility measurements on polycrystalline samples of **1** and **2** were made by using a Quantum Design MPMS SQUID magnetometer equipped with a 5.5 T magnet and operating in the range 2.5−300 K. The susceptibilities of the sample holder were measured at the same fields and temperatures for an accurate assessment of its contribution to the total measured susceptibility. Diamagnetic corrections were estimated from Pascal's constants[41,42] and subtracted from the experimental susceptibilities. AC susceptibility measurements on polycrystalline samples of **1**−**3** were made with a home-built susceptometer operating at 98 Hz and capable of reaching temperatures as low as 1.4 K. DC magnetic measurements on a single crystal of **3** were made by using a Metronique MS02 SQUID magnetometer operating between 2 and 300 K.

High-Field Magnetization Studies. Solid state magnetization measurements on polycrystalline samples of **1** and **2** were made with a vibrating-sample (Foner) magnetometer at the Francis Bitter National Magnet Laboratory. Electronics were modified for use in Bitter magnets. Sample holders were made from Teflon or Kel-F and fitted with plungers that allowed for compression of the powders by hand to prevent mechanical torquing in the applied field. Data were collected between 0 and 200 kOe for all samples.

(33) Tracer In Lawton, S. L. *TRACER II, A Fortran Transformation-Cell Reduction Program*; Mobil Oil Corp.: Paulsboro, NJ, 1967.

(34) North, A. C. T.; Phillips, D. C.; Mathews, F. S. *Acta Crystallogr.* **1968**, *A24*, 351−359.

(35) Burla, M. C.; Camalli, M.; Cascarano, G.; Giacovazzo, C.; Polidori, G.; Spagna, R.; Viterbo, D. *J. Appl. Crystallogr.* **1989**, *22*, 389−393.

(36) Cromer, D. T.; Waber, J. T. *International Tables for X-ray Crystallography;* Kynoch Press: Birmingham, U.K., 1974; Vol. 4, pp 71−98.

(37) Stewart, R. F.; Davidson, E. R.; Simpson, W. T. *J. Chem. Phys.* **1965**, *42*, 3175−3187.

(38) Ibers, J. A.; Hamilton, W. C. *Acta Crystallogr.* **1964**, *17*, 781−782.

(39) Creagh, D. C.; McAuley, W. J. *International Tables for X-ray Crystallography;* Kluwer Academic Publishers: Dordrecht, The Netherlands, 1992; Vol. C, pp 219−222.

(40) *Single Crystal Structure Analysis Software*, Version 1.6; Molecular Structure Corp.: The Woodlands, TX, 1993.

(41) Carlin, R. L. *Magnetochemistry*; Springer-Verlag: New York, 1986.

(42) O'Connor, C. J. *Prog. Inorg. Chem.* **1982**, *29*, 203−283.

Table 2. Selected Bond Lengths (Å) and Angles (deg) for $[Me_4N]_4[Mn_{10}O_4(biphen)_4Br_{12}]\cdot 4CH_3CN\cdot 0.5H_2O$ ($2\cdot 4CH_3CN\cdot 0.5H_2O$)[a]

(a) Distances

Mn(1)−Br(3)	2.734(5)	Mn(4)−Br(10)	2.609(5)	Mn(7)−O(5)	2.18(1)
Mn(1)−Br(6)	2.730(5)	Mn(4)−O(2)	2.13(1)	Mn(8)−Br(1)	2.752(5)
Mn(1)−Br(10)	2.681(5)	Mn(4)−O(4)	2.18(2)	Mn(8)−Br(2)	2.663(5)
Mn(1)−Br(12)	2.649(5)	Mn(4)−O(8)	2.13(1)	Mn(8)−Br(4)	2.755(5)
Mn(1)−O(4)	2.14(2)	Mn(5)−Br(3)	2.850(5)	Mn(8)−Br(5)	2.689(5)
Mn(1)−O(12)	2.15(2)	Mn(5)−Br(4)	2.812(4)	Mn(8)−O(5)	2.15(1)
Mn(2)−Br(1)	2.859(5)	Mn(5)−O(7)	1.94(1)	Mn(8)−O(10)	2.13(1)
Mn(2)−Br(3)	2.839(5)	Mn(5)−O(9)	1.91(2)	Mn(9)−Br(9)	2.493(5)
Mn(2)−O(4)	1.88(2)	Mn(5)−O(10)	1.88(1)	Mn(9)−Br(12)	2.596(5)
Mn(2)−O(8)	1.95(1)	Mn(5)−O(12)	1.90(2)	Mn(9)−O(6)	2.16(1)
Mn(2)−O(10)	1.90(1)	Mn(6)−Br(5)	2.626(5)	Mn(9)−O(7)	2.14(1)
Mn(2)−O(11)	1.92(2)	Mn(6)−Br(8)	2.482(5)	Mn(9)−O(12)	2.20(1)
Mn(3)−Br(1)	2.830(5)	Mn(6)−O(9)	2.14(2)	Mn(10)−Br(4)	2.850(5)
Mn(3)−Br(6)	2.823(4)	Mn(6)−O(10)	2.22(1)	Mn(10)−Br(6)	2.840(5)
Mn(3)−O(2)	1.94(2)	Mn(6)−O(11)	2.16(2)	Mn(10)−O(1)	1.95(2)
Mn(3)−O(3)	1.93(1)	Mn(7)−Br(2)	2.596(5)	Mn(10)−O(5)	1.91(1)
Mn(3)−O(4)	1.91(1)	Mn(7)−Br(11)	2.520(5)	Mn(10)−O(6)	1.90(1)
Mn(3)−O(5)	1.88(1)	Mn(7)−O(1)	2.16(1)	Mn(10)−O(12)	1.88(1)
Mn(4)−Br(7)	2.469(5)	Mn(7)−O(3)	2.17(1)		

(b) Angles

Br(3)−Mn(1)−Br(6)	163.7(2)	O(2)−Mn(4)−O(4)	73.5(6)	Br(5)−Mn(8)−O(10)	86.2(4)
Br(3)−Mn(1)−Br(10)	97.2(1)	O(2)−Mn(4)−O(8)	125.9(6)	O(5)−Mn(8)−O(10)	90.3(5)
Br(3)−Mn(1)−Br(12)	96.6(1)	O(4)−Mn(4)−O(8)	73.7(5)	O(7)−Mn(9)−O(12)	73.4(6)
Br(6)−Mn(1)−Br(10)	93.3(1)	Br(4)−Mn(5)−O(10)	87.2(4)	Br(9)−Mn(9)−Br(12)	109.2(2)
Br(6)−Mn(1)−Br(12)	94.3(1)	Br(4)−Mn(5)−O(12)	83.2(5)	Br(9)−Mn(9)−O(6)	103.3(4)
Br(10)−Mn(1)−Br(12)	98.0(1)	O(7)−Mn(5)−O(9)	93.8(6)	Br(9)−Mn(9)−O(7)	98.1(4)
Br(3)−Mn(1)−O(12)	84.6(4)	O(7)−Mn(5)−O(10)	176.0(6)	Br(9)−Mn(9)−O(12)	164.5(5)
Br(6)−Mn(1)−O(4)	84.1(4)	O(7)−Mn(5)−O(12)	84.9(6)	Br(12)−Mn(9)−O(6)	108.0(5)
Br(6)−Mn(1)−O(12)	84.1(4)	O(9)−Mn(5)−O(10)	84.8(6)	Br(12)−Mn(9)−O(7)	113.2(4)
Br(6)−Mn(1)−O(12)	84.1(4)	O(9)−Mn(5)−O(12)	176.1(7)	Br(12)−Mn(9)−O(12)	86.3(4)
Br(10)−Mn(1)−O(4)	85.7(4)	O(10)−Mn(5)−O(12)	96.7(6)	O(6)−Mn(9)−O(7)	123.4(6)
Br(10)−Mn(1)−O(12)	175.5(4)	Br(3)−Mn(5)−Br(4)	164.0(2)	O(6)−Mn(9)O(12)	72.3(5)
Br(12)−Mn(1)−O(4)	176.1(4)	Br(3)−Mn(5)−O(7)	94.0(4)	Br(4)−Mn(10)−Br(6)	162.2(1)
Br(12)−Mn(1)−O(12)	85.9(4)	Br(3)−Mn(5)−O(9)	97.9(5)	Br(6)−Mn(10)−O(1)	98.7(5)
O(4)−Mn(1)−O(12)	90.4(6)	Br(3)−Mn(5)−O(10)	82.5(4)	Br(6)−Mn(10)−O(5)	82.1(4)
Br(1)−Mn(2)−Br(3)	162.9(1)	Br(3)−Mn(5)−O(12)	85.9(5)	Br(6)−Mn(10)−O(6)	93.5(5)
Br(1)−Mn(2)−O(4)	82.6(5)	Br(4)−Mn(5)−O(7)	96.7(4)	Br(6)−Mn(10)−O(12)	85.9(5)
Br(1)−Mn(2)−O(8)	99.2(5)	Br(4)−Mn(5)−O(9)	93.3(5)	O(1)−Mn(10)−O(5)	85.9(6)
Br(1)−Mn(2)−O(10)	86.0(4)	Br(5)−Mn(6)−Br(8)	114.6(2)	O(1)−Mn(10)−O(6)	92.6(6)
Br(1)−Mn(2)−O(11)	93.5(5)	Br(5)−Mn(6)−O(9)	108.8(5)	Br(4)−Mn(10)−O(1)	93.6(5)
Br(3)−Mn(2)−O(4)	86.2(5)	Br(5)−Mn(6)−O(10)	86.0(4)	Br(4)−Mn(10)−O(5)	86.0(4)
Br(3)−Mn(2)−O(8)	92.6(5)	Br(5)−Mn(6)−O(11)	109.6(4)	Br(4)−Mn(10)−O(6)	98.8(5)
Br(3)−Mn(2)−O(10)	82.4(4)	Br(8)−Mn(6)−O(9)	98.3(4)	Br(4)−Mn(10)−O(12)	82.4(5)
Br(3)−Mn(2)−O(11)	98.3(5)	Br(8)−Mn(6)−O(10)	159.4(4)	O(1)−Mn(10)−O(12)	175.1(7)
O(4)−Mn(2)−O(8)	84.9(6)	Br(8)−Mn(6)−O(11)	99.6(5)	O(5)−Mn(10)−O(6)	175.1(7)
O(4)−Mn(2)−O(10)	96.3(6)	O(9)−Mn(6)−O(10)	72.0(6)	O(5)−Mn(10)O(12)	96.6(6)
O(4)−Mn(2)−O(11)	174.9(7)	O(9)−Mn(6)−O(11)	125.2(6)	O(6)−Mn(10)−O(12)	85.3(6)
O(8)−Mn(2)−O(10)	174.8(6)	O(10)−Mn(6)−O(11)	73.4(5)	Mn(1)−O(4)−Mn(3)	112.8(7)
O(8)−Mn(2)−O(11)	92.6(6)	Br(2)−Mn(7)−Br(11)	108.6(2)	Mn(1)−O(4)−Mn(4)	106.0(7)
O(10)−Mn(2)−O(11)	86.6(6)	Br(2)−Mn(7)−O(1)	108.9(4)	Mn(2)−O(4)−Mn(3)	120.7(8)
Br(6)−Mn(3)−O(3)	97.3(5)	Br(2)−Mn(7)−O(3)	113.4(4)	Mn(2)−O(4)−Mn(4)	100.5(7)
Br(6)−Mn(3)−O(4)	85.8(5)	Br(2)−Mn(7)−O(5)	86.8(4)	Mn(3)−O(4)−Mn(4)	100.5(7)
Br(6)−Mn(3)−O(5)	83.1(4)	Br(11)−Mn(7)−O(1)	103.1(4)	Mn(1)−O(4)−Mn(2)	113.3(7)
O(2)−Mn(3)−O(3)	93.7(6)	Br(11)−Mn(7)−O(3)	96.8(4)	Mn(3)−O(5)−Mn(7)	101.7(6)
O(2)−Mn(3)−O(4)	84.1(7)	Br(11)−Mn(7)−O(5)	164.1(4)	Mn(3)−O(5)−Mn(8)	112.5(7)
O(2)−Mn(3)−O(5)	175.8(7)	O(1)−Mn(7)−O(3)	123.7(6)	Mn(3)−O(5)−Mn(10)	120.9(7)
O(3)−Mn(3)−O(4)	176.3(7)	O(1)−Mn(7)−O(5)	74.7(5)	Mn(7)−O(5)−Mn(8)	105.6(6)
O(3)−Mn(3)−O(5)	84.8(6)	O(3)−Mn(7)−O(5)	72.6(5)	Mn(7)−O(5)−Mn(10)	100.0(6)
O(4)−Mn(3)−O(5)	97.6(6)	Br(1)−Mn(8)−Br(2)	98.2(1)	Mn(8)−O(5)−Mn(10)	113.1(6)
Br(1)−Mn(3)−Br(6)	164.0(2)	Br(1)−Mn(8)−Br(4)	164.0(2)	Mn(5)−O(10)−Mn(6)	100.2(6)
Br(1)−Mn(3)−O(2)	97.0(5)	Br(1)−Mn(8)−Br(5)	94.7(1)	Mn(5)−O(10)−Mn(8)	112.9(6)
Br(1)−Mn(3)−O(3)	94.3(5)	Br(1)−Mn(8)−O(5)	84.3(4)	Mn(6)−O(10)−Mn(8)	106.2(6)
Br(1)−Mn(3)−O(4)	83.0(5)	Br(1)−Mn(8)−O(10)	84.8(4)	Mn(2)−O(10)−Mn(5)	121.6(7)
Br(1)−Mn(3)−O(5)	87.1(4)	Br(2)−Mn(8)−Br(4)	92.0(1)	Mn(2)−O(10)−Mn(6)	98.9(6)
Br(6)−Mn(3)−O(2)	93.2(5)	Br(2)−Mn(8)−Br(5)	97.9(1)	Mn(2)−O(10)−Mn(8)	113.5(7)
Br(7)−Mn(4)−Br(10)	109.5(2)	Br(2)−Mn(8)−O(5)	85.6(4)	Mn(1)−O(12)−Mn(5)	113.0(7)
Br(7)−Mn(4)−O(2)	98.9(4)	Br(2)−Mn(8)−O(10)	174.7(4)	Mn(1)−O(12)−Mn(9)	105.4(6)
Br(7)−Mn(4)−O(4)	163.6(5)	Br(4)−Mn(8)−Br(5)	96.1(1)	Mn(1)−O(12)−Mn(10)	113.6(8)
Br(7)−Mn(4)−O(8)	100.7(4)	Br(4)−Mn(8)−O(5)	84.3(4)	Mn(5)−O(12)−Mn(9)	100.3(7)
Br(10)−Mn(4)−O(2)	109.3(4)	Br(4)−Mn(8)−O(10)	84.2(4)	Mn(5)−O(12)−Mn(10)	120.8(8)
Br(10)−Mn(4)−O(4)	86.8(4)	Br(5)−Mn(8)−O(5)	176.4(4)	Mn(9)−O(12)−Mn(10)	100.5(7)
Br(10)−Mn(4)−O(8)	110.5(4)				

[a] For atom-labeling scheme, see Figure 1. Estimated standard deviations in the least significant figure are given in parentheses.

EPR Studies. A Varian E-9 spectrometer equipped with an Oxford Instruments EPR 9 liquid helium continuous flow cryostat was used to collect both polycrystalline and single-crystal EPR spectra.

Results and Discussion

Synthesis and Composition of the $[Mn_{10}O_4(biphen)_4Cl_{12}]^{4-}$ Cluster. The preparation of the $[Mn_{10}O_4(biphen)_4Cl_{12}]^{4-}$ anion was accomplished by addition of Me_4NOH as a source of base to a solution of $MnCl_2$ and biphenH_2 in EtOH. Layering of the filtered reaction mixture over CH_2Cl_2 gave X-ray quality crystals of **1**. Subsequent determination of the structure of **1** by X-ray crystallography revealed the geometry of the Mn_{10} anion, but satisfactory refinement was precluded by disorder of solvent molecules, most likely CH_2Cl_2, in the crystal lattice. A second structure of better quality was obtained on crystals of **1** grown by layering of benzene onto the filtered reaction mixture and was reported elsewhere.[32] The utility of the EtOH/C_6H_6 solvent system was limited by the cocrystallization of a white product with the red-brown crystals of **1**, making the EtOH/CH_2Cl_2 system the one of choice for bulk preparation.

The mixed-valent cluster has four Mn(III) and six Mn(II) ions, the oxidizing agent necessary for the generation of the Mn(III) centers most likely being atmospheric dioxygen. The redox reaction is initiated by the addition of base, as evidenced by the immediate formation of the dark brown color. A formal balanced equation for the synthesis of **1** and **2** can be written as indicated in eq 1. One-electron reduction of dioxygen by

$$10MnX_2 + 4biphenH_2 + 12OH^- + O_2 \rightarrow [Mn_{10}O_4(biphen)_4X_{12}]^{4-} + 8X^- + 10H_2O \quad (1)$$

four Mn(II) ions would generate the appropriate number of Mn(III) ions and two of the four O^{2-} ligands. The deprotonation of two OH^- ions would provide the other two O^{2-} ligands. This equation should be taken only as an intriguing formalism, given the difficulty in determining the actual mechanism of assembly of such a large polynuclear cluster. We made no attempt to establish the source of the oxo ligands or to control the O_2 stoichiometry during the preparation of **1** or **2**.

Given the critical role of the halide ion in assembling the structure of the Mn_{10} cluster, we wondered whether it would be possible to substitute Br^- for Cl^- and maintain the structural integrity of the complex. The structural framework of **1** would have to undergo a significant expansion upon substitution of the larger Br^- (ionic radius = 1.96 Å) for Cl^- (ionic radius = 1.81 Å) ion.[43] Moreover, very few well characterized, higher valent ($\geq +3$) Mn compounds are known with Br^- as a ligand, possibly because of redox instability.[8,44,45] Despite these potential barriers, the preparation of the bromide derivative **2** was accomplished with relative ease, simply by substitution of $MnBr_2$ for $MnCl_2$.

Preparation of the analogous bromide derivative in a manner identical to that for **1** gave crystalline **2**, which analyzed well for the corresponding Mn_{10} cluster.[32] X-ray quality crystals of **2** were grown by vapor diffusion of toluene into acetonitrile. The structure is described below. Since $MnBr_2$ is more soluble in CH_3CN than $MnCl_2$, compound **2** was prepared by using acetonitrile as the solvent instead of EtOH.

In order to explore the generality of the Mn_{10} complex synthesis, we attempted to prepare the cluster by addition of an exogenous base other than Me_4NOH. Such a substitution would allow us to determine whether the redox reaction necessary to form the mixed-valent cluster could occur in the presence of a base other than hydroxide ion and to establish whether the $[Mn_{10}O_4(biphen)_4X_{12}]^{4-}$ anion could be assembled with a cation other than Me_4N^+. When Et_3N was employed as the base, compound **3** was obtained. The same dark red-brown color noted in the reaction with Me_4NOH appeared immediately upon addition of Et_3N. Structural characterization of **3** by X-ray crystallography revealed the presence of the same Mn_{10} cluster as in **1** and **2**, but with Et_3NH^+ and mononuclear Mn(II) cations in the lattice.[46] Single crystals of **3** had tetragonal morphology, consistent with the Laue symmetry of the compound. When the scale of the reaction was reduced 4-fold, including the solvent volume, dark red-brown crystals having a rectangular, block-shaped morphology cocrystallized with **3**. The unit cell of these block-shaped crystals was determined to be orthorhombic,[47] but they were not of sufficient quality to afford a good structure determination. Upon increasing the concentration of reagents by a factor of 4, only the orthorhombic crystals formed. Crystals of **3** were readily separated under a microscope by hand from the orthorhombic material, owing to their clearly distinguishable morphology, and identified conclusively by a unit cell determination. The synthesis described in the Experimental Section yields only the tetragonal-shaped crystals of **3**, but a systematic investigation of the effects of varying the concentration of reagents in the synthesis of **3** was not carried out, so one must be aware that the orthorhombic material might form as a potential impurity. Further details of this work are reported elsewhere.[46] The high-symmetry space group of **3** was important for deconvoluting the magnetic behavior of the Mn_{10} unit because it allowed for the collection and easy interpretation of both single-crystal susceptibility and EPR measurements.

When stored under an inert atmosphere at room temperature, compound **3** loses crystallinity owing to solvent loss. If crystals of **3** are allowed to stand in air for a few weeks, they decompose to give an amorphous material, as shown by the absence of a powder diffraction pattern. A variable-temperature magnetic susceptibility study of this product revealed a magnetic phase transition at ≈40 K, very similar to that observed for hausmannite (Mn_3O_4).[48,49] It is therefore possible that at least a portion of the material, most likely the Mn(II) cations, was being oxidized upon prolonged exposure to air to give this mineral. Successive washing with acetone, CH_3CN, and EtOH led to the isolation of a pure inorganic compound which retained the magnetic phase transition near 40 K. This material was 70% manganese by weight, as determined by atomic absorption spectroscopy, close to the manganese composition of Mn_3O_4 (72.03%). The yield of material obtained by this procedure is approximately 10% based on the manganese content of **3**.

Molecular Structures. $[Me_4N]_4[(Mn_{10}O_4(biphen)_4Br_{12}]$ (2). An ORTEP diagram of $[(Mn_{10}O_4(biphen)_4Br_{12}]^{4-}$ is shown in Figure 1. This complex has the same overall structure as the chloride derivative **1**. An adamantane-like inner core is formed by Mn(5), O(10), Mn(8), O(5), Mn(10), O(12), Mn(1), Mn(2), Mn(3), and O(4), with Mn(1) and Mn(8) being the two inner Mn(II) ions. The μ_4-oxo ligands, O(4), O(5), O(10), and O(12), are each bound to an outer Mn(II) ion, Mn(4), Mn(7), Mn(6), and Mn(9), respectively. The four Mn(III) ions are easily distinguished as the metal ions chelated by the four biphenoxide ligands. Each biphenoxide oxygen atom bridges a Mn(III) ion and an outer Mn(II) ion. The 12 bromide ligands in the cluster are bound in three different modes. Four bromide

(43) Shannon, R. D. *Acta Crystallogr., Sect. A* **1976**, *32*, 751–767.
(44) Morris, R. J.; Girolami, G. S. *Organometallics* **1987**, *6*, 1815–1816.
(45) Bryan, P. S.; Dabrowiak, J. C. *Inorg. Chem.* **1975**, *14*, 296–299.
(46) Goldberg, D. P. Ph.D. Thesis, Massachusetts Institute of Technology, 1994.
(47) Unit cell parameters: $a = 15.832(8)$, $b = 18.923(8)$, $c = 36.223(8)$.
(48) Srinivasan, G.; Seeline, M. S. *Phys. Rev. B* **1983**, *28*, 1–7.
(49) Dwight, K.; Menyuk, N. *Phys. Rev.* **1960**, *119*, 1470–1479.

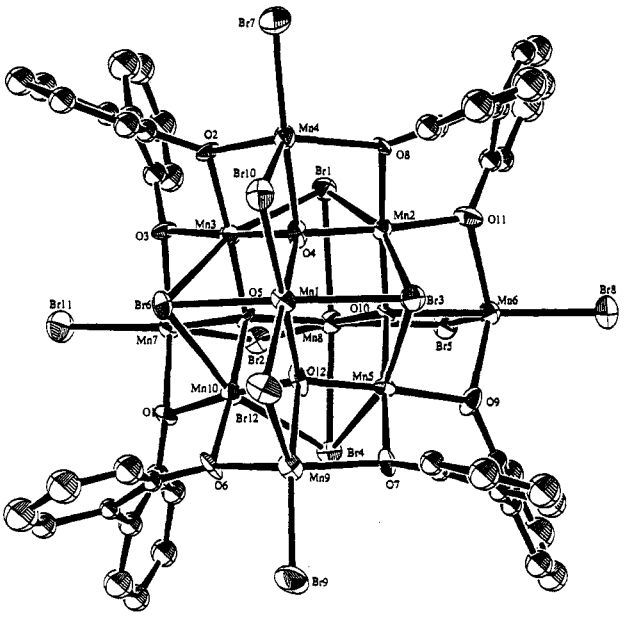

Figure 1. ORTEP diagram showing the anion of $[Me_4N]_4[Mn_{10}O_4(biphen)_4Br_{12}]$ (**2**) with 50% probability thermal ellipsoids. Hydrogen atoms have been omitted for clarity.

ions, Br(3), Br(6), Br(4), and Br(1), each bridge three metal ions. Four other bromide ions are bound in a doubly-bridging mode between two linear arrays of metal ions, Mn(9), Mn(1), and Mn(4) along the front vertical edge and Mn(6), Mn(8), and Mn(7) along the back horizontal edge of the cluster. The remaining bromide ions are coordinated in a terminal fashion to the outer Mn(II) ions.

The structure of compounds **1** and **2** bears a striking resemblance to a series of metal chalcogenide cluster complexes of formulas $[E_4M_{10}(E'R)_{16}]^{4-}$ and $[E_4M_{10}(E'R)_{12}X_4]^{4-}$, with E, E′ = S, Se, or Te, M = Zn or Cd, and X = Cl, Br, or I.[50-52] These compounds comprise four fused adamantane cages, and their metal atoms form a framework very similar to that of **1** and **2**, although the metal sites have exclusively tetrahedral geometries. An even closer structural relationship to **1** and **2** is found for a thiostannate cluster complex of composition $[Sn_{10}O_4S_{20}]^{8-}$,[53] which contains four μ_3-oxo ligands at the center of each adamantane cage. The positions of the oxo bridges within the Sn_{10} framework are identical to those of the μ_4-oxo ligands in **1** and **2**. The thiostannate polyanion would have a core structure *identical* to those of **1** and **2** if the oxo ligands were bonded to the fourth closest metal site.

Oxidation states for the manganese ions in **1** and **2** are readily assigned by examining the bond distances for the first coordination sphere of each metal. Many compounds containing Mn(III) ions exhibit the classic Jahn–Teller distorted geometry expected for a d^4 ion, making the identification of this oxidation state for manganese straightforward. As can be seen in Figure 1, the Mn(III) ions Mn(2), Mn(3), Mn(5), and Mn(10) have an octahedral environment with a Br_2O_4 donor set, and Table 2 clearly reveals that the bromide ligands occupy axially-elongated sites, with an average Mn–Br distance of 2.84 Å. As one might expect, the Mn(III) ions are coordinated by the hardest set of ligand donor atoms, Br_2O_4, which corresponds to the highest O/Br ratio among the metal ions.

(50) Dance, I.; Fisher, K. *Prog. Inorg. Chem.* **1994**, *41*, 637–803.
(51) Krebs, B.; Henkel, G. *Angew. Chem., Int. Ed. Engl.* **1991**, *30*, 769–788.
(52) Dance, I. G.; Choy, A.; Scudder, M. L. *J. Am. Chem. Soc.* **1984**, *106*, 6285–6295.
(53) Schiwy, W.; Krebs, B. *Angew. Chem., Int. Ed. Engl.* **1975**, *14*, 436.

As shown in Table 3, the average distances of the oxygen ligands to the Mn(III) sites in **1** and **2** are significantly shorter than the Mn–O distances for the Mn(II) atoms. The manganese(II) atoms Mn(1) and Mn(8) have octahedral geometries, whereas the remaining Mn(II) ions are bound in distorted trigonal bipyramidal sites.

To our knowledge, only two other compounds containing Mn(III)–Br bonds have been characterized by X-ray crystallography, one of which is $[Mn_4O_3Br(OAc)_3(dbm)_3]$ (dbmH = dibenzoylmethane),[8] an $Mn(III)_3Mn(IV)$ complex with a distorted cubane structure. The bromide ligand in this molecule bridges three octahedral manganese(III) atoms and occupies an elongated axial position on each Jahn–Teller distorted Mn(III) site. The average Mn–Br distance in this compound is 2.803 Å, nearly identical to that in **2**. The other structurally characterized Mn(III)Br compound is $Mn(C_6H_2Me_3)Br_2(PMe_3)_2$,[44] a high-spin organomanganese(III) complex with a distorted trigonal bipyramidal geometry. The bromide ligands occupy equatorial positions, with a significantly shorter average Mn–Br distance of 2.50 Å, as expected in the absence of a Jahn–Teller distortion. Compound **2** is only the second example where a Br^- ion bridges Mn(III) centers, the first being the $Mn(III)_3$-Mn(IV) complex.

The lengthening of the Mn–halide bonds on going from Cl^- to Br^- is approximately 0.13–0.15 Å for all manganese centers in **1** and **2**, as can be seen in Table 3. This increase is in excellent agreement with the difference in the ionic radii of Br^- and Cl^-, 0.15 Å.[43]

$[Et_3NH]_2[Mn(CH_3CN)_4(H_2O)_2][Mn_{10}O_4(biphen)_4Br_{12}]$ (3). The crystal structure of **3** reveals an Mn_{10} complex that is isostructural with the anion in **2**. Although we encountered difficulties in refining the lattice solvent and counterions which remain unresolved and prevent us from presenting the structure in detail here, the metrical data for the Mn_{10} cluster of **3** are in excellent agreement with those of **2**, giving us confidence that the clusters are identical.[46] The complex anion resides at a special position of $\bar{4}$ site symmetry in space group *I*4/*m*, making only one-quarter of the atoms in the cluster unique. The remaining atoms in the anion are generated by the crystallographically-imposed S_4 axis, giving the complex strict D_{2d} symmetry. One of the manganese ions, Mn(3), resides on a crystallographically-imposed 2-fold axis. The $[Mn_{10}O_4(biphen)_4Br_{12}]^{4-}$ units are stacked in an eclipsed fashion along the S_4 axes, running parallel with the *c* axis. A packing diagram is shown in Figure 2 to highlight this stacking arrangement.

Powder Magnetic Studies. A plot of the product of the molar magnetic susceptibility versus temperature for powdered samples of **1** and **2** is shown in Figure 3. The previously published[32] susceptibility data for **1** are included for comparison. Substitution of Br^- for Cl^- ions clearly has no affect on the overall magnetic properties of the cluster. The χT curve for **2** steadily increases from 37.9 emu mol^{-1} K at 300 K, very close to the 38.2 emu mol^{-1} K value expected if all of the manganese spins are uncorrelated, to 95.1 emu mol^{-1} K at 5 K. Measurements performed on **1** between 300 and 400 K reveal that χT decreases below the value expected for the uncorrelated spins, reaching 35 emu mol^{-1} K near 400 K (data not shown). As found for **1**, the low-temperature χT product lies between the theoretical values calculated for $S = 13$ ($\chi T_{calcd} = 91$ emu mol^{-1} K) and $S = 14$ ($\chi T_{calcd} = 105$ emu mol^{-1} K) ground states, assuming an average *g* value of 2.0 for the cluster.

The insets of Figure 3a,b show the reduced magnetization data for **1** and **2** at 4.2 K as a function of magnetic field up to 200 kOe. The magnetization curves for **1** and **2** increase rapidly at low field and reach a plateau at the higher fields, with final

Table 3. Average Bond Distances for Compounds **1** and **2**[b]

Mn oxidn state	geom[a]	donor set (X = Cl^-, Br^-)	compd **1** Mn−O_{av} (Å)	compd **2** Mn−O_{av} (Å)	compd **1** Mn−Cl_{av} (Å)	compd **2** Mn−Br_{av} (Å)
Mn(II)	tbp	X_2O_3	2.18(2)	2.16(3)	2.40(7)	2.55(6)
Mn(II)	oct	X_4O_2	2.14(1)	2.14(1)	2.56(6)	2.71(4)
Mn(III)	oct	X_2O_4	1.91(2)	1.91(3)	2.71(3)	2.84(2)

[a] tbp = trigonal bipyramidal; oct = octahedral. [b] Values in parentheses are the standard deviations on the averaged parameters.

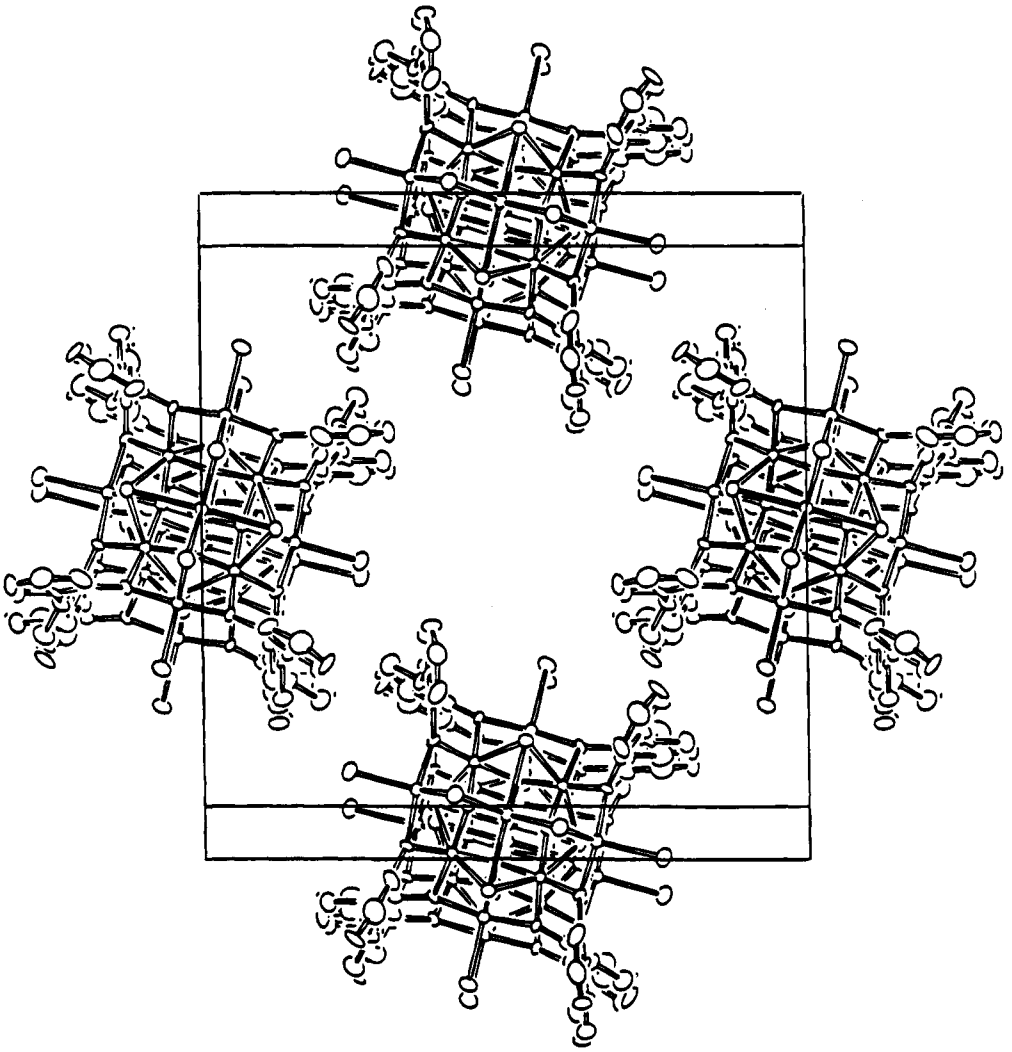

Figure 2. Packing diagram showing non-hydrogen atoms of the anion of $[Et_3NH]_2[Mn(CH_3CN)_4(H_2O)_2][Mn_{10}O_4(biphen)_4Br_{12}]$ (**3**).

saturation values of 27.1 and 28.3 μ_B for **1** and **2**, respectively. By using the simple relation $M_{sat}/N\mu_B = gS$, and assuming g = 2.0, a ground state near S = 14 is indicated for both **1** and **2**. The close similarity in the magnetic behaviors of **1** and **2** suggests that the magnetic exchange interactions are little influenced by the bridging halide ions.

The magnetic susceptibility for a powdered sample of **3**, shown in Figure 4, exhibits behavior similar to that of **1** and **2**. The χT product steadily increases as the temperature is lowered, from a value at 300 K of χT = 43 emu mol^{-1} K to a maximum of χT = 82 emu mol^{-1} K near 10 K. This value corresponds to an S = 12 ground state taking g = 2.0 and including the contribution of the isolated $S = {}^5/_2$ Mn(II) cation. The observation that a similar maximum is not reached in the χT vs T plots for compounds **1** and **2** might be ascribed to the presence of stronger intercluster magnetic interactions in these compounds as compared to **3**. Such interactions are expected to be very weak, however, being mainly dipolar in nature, since there are no evident superexchange pathways between clusters. Another explanation for the lack of a maximum may be the presence of states of varying large spin multiplicity lying close in energy to the ground state.

The magnetic susceptibilities of **1**−**3** were measured in zero applied field down to temperatures as low as 1.4 K by the use of an AC susceptometer. In all cases, paramagnetic behavior, with no imaginary component of the AC susceptibility, was observed.

Single-Crystal Magnetic Studies. The tetragonal symmetry of compound **3** and the macroscopic morphology of the crystals made it an excellent candidate for anisotropy measurements. Only two measurements, parallel and perpendicular to the unique axis, were necessary to determine the anisotropy tensor. The χT vs T curves for a single crystal of **3** with the applied magnetic field oriented parallel and perpendicular to the crystallographic c axis are shown in Figure 4. In the parallel orientation, $\chi_{\parallel}T$ rapidly increased to a value of 128 emu mol^{-1} K at 2.2 K. When the external field was applied perpendicular to the c axis, $\chi_{\perp}T$ reached a broad maximum of 80 emu mol^{-1} K near 15 K, followed by a decrease to 46 emu mol^{-1} K at 2.1 K. The calculated powder-average value of χT, using the relation χT_{av}

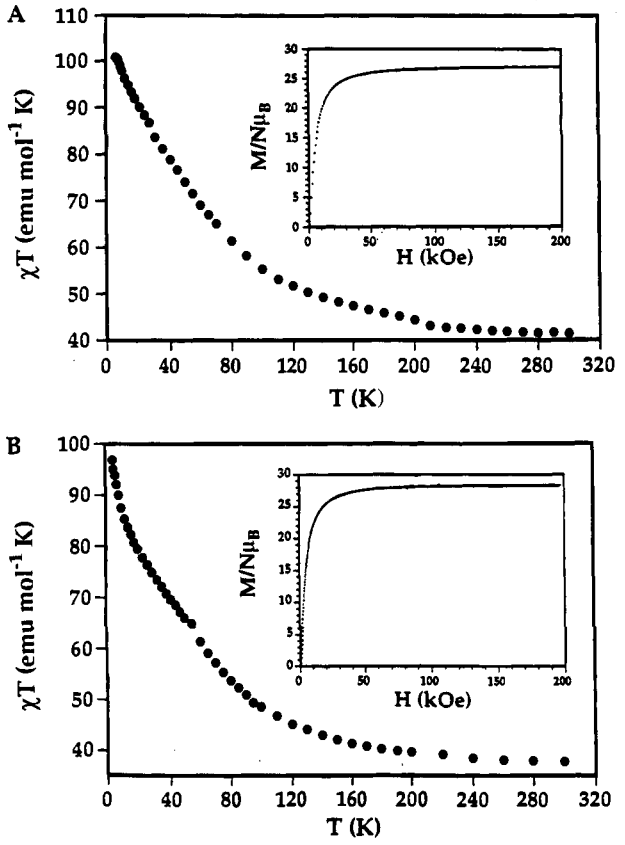

Figure 3. (A) Plot of the product of the temperature times molar susceptibility versus temperature for **1**. Inset: Plot of the reduced magnetization versus field, where N is Avogadro's number and μ_B is the Bohr magneton, at 4.2 K for **1**. (B) Plot of the product of the temperature times molar susceptibility versus temperature for **2**. Inset: Plot of the reduced magnetization versus field, where N is Avogadro's number and μ_B is the Bohr magneton, at 4.2 K for **2**.

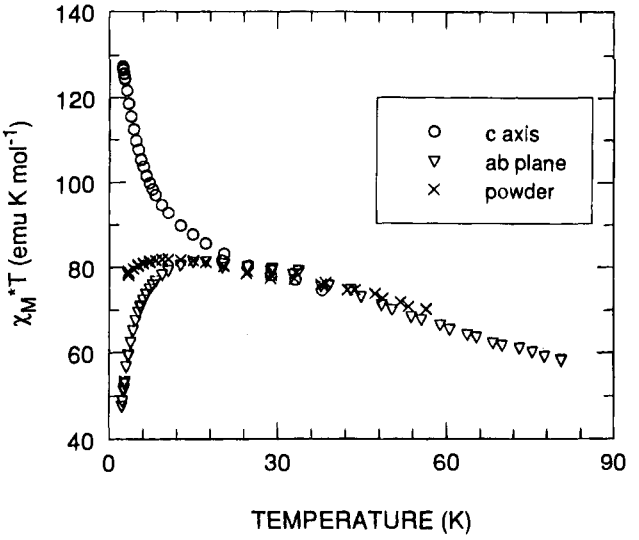

Figure 4. Plot of the product of the temperature times molar susceptibility versus temperature for **3** on a powder sample (×), a single crystal with the applied field parallel (○) and perpendicular (▽) to the tetragonal c axis. H = 1000 Oe.

= $1/3(2\chi_\perp T + \chi_\parallel T)$ was 74 emu mol^{-1} K at 2.2 K, in good agreement with the observed value of 77 emu mol^{-1} K at this temperature. The system clearly exhibits an Ising-type anisotropy, with one axis of favorite magnetization and a hard plane, which cannot be attributed to **g** anisotropy owing to its large temperature dependence.

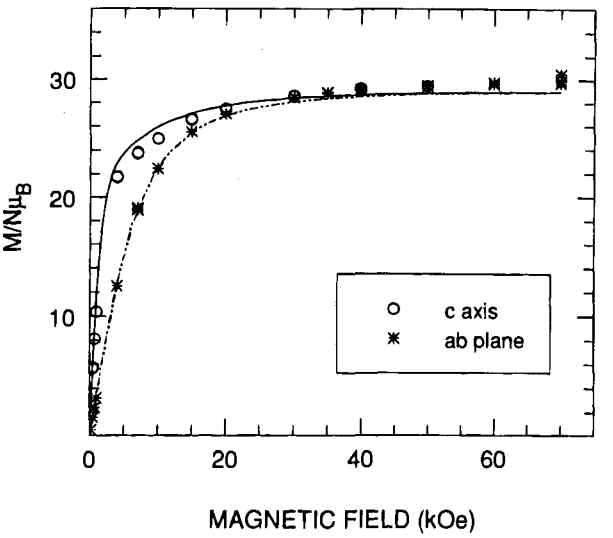

Figure 5. Plot of the reduced magnetization versus field for a single crystal of **3** at 2 K with the applied field parallel (○) and perpendicular (*) to the tetragonal c axis. The solid and dashed lines correspond to the simulated curve for an S = 12 system with g = 2.0 and D = −0.035 cm^{-1}, including a simple Brillioun function taking into account the paramagnetic contribution from the isolated $S = {}^5/_2$ Mn(II) cation.

The saturation magnetization measured at 2 K for a single crystal of **3**, with the applied field parallel or perpendicular to the c axis, is shown in Figure 5. As evident from the plot, the reduced magnetization increased much more rapidly when the field was applied parallel to the c axis. Above approximately 30 kOe, the two curves became equal and the reduced magnetization smoothly increased to a value near 29 μ_B at maximum field.

EPR Spectroscopy. The X-band EPR spectrum at room temperature of a powdered sample of **3** exhibited a broad, structureless line at g = 2.0 with ΔH_{pp} = 750 G. Upon lowering of the temperature to 4.2 K, a complex spectrum arose, with signals being observed up to 10 kG, a result that is difficult to interpret. The X-band spectrum of a single crystal of **3** at room temperature indicated that the linewidth of this broad g = 2.0 feature depended on the orientation of the crystallographic axes and the direction of the applied magnetic field, with ΔH_{pp} = 1020 G when the c axis was held parallel to the applied field and ΔH_{pp} = 650 G when the field lay in the *ab* plane.

At temperatures below 70 K, a complex pattern in the EPR spectrum of a single crystal of **3** was resolved, irrespective of the magnetic field orientation. The EPR spectrum for a single crystal of **3** at liquid helium temperature with the field oriented parallel to the c axis is shown in Figure 6. A signal centered at g = 2.0 (3300 G) complicated the analysis of this spectrum, but some critical features were apparent. In the high-field region ($H \geq$ 5000 G), nine equally spaced lines with intensity decreasing as the field increases were observed. The resonance of weakest intensity was found near 11 800 G. The separation between these resonances was approximately 750 G.

Theoretical Analysis. A high-spin ground state of multiplicity $12 \leq S \leq 14$ is supported by all of the powder susceptibility and high-field magnetization data for compounds **1** and **2**. An exact theoretical fit of the susceptibility data is simply not possible because the dimensions of the spin Hamiltonian matrix for a system comprising six $S = {}^5/_2$ and four S = 2 spins are far too large to be handled by standard computing facilities, even with reductions in the size of the matrices brought about

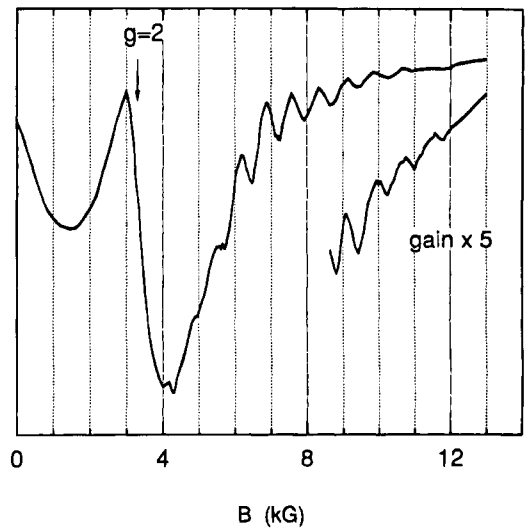

Figure 6. X-Band EPR spectrum of a single crystal of **3** at 4.2 K with the static magnetic field oriented parallel to the tetragonal *c* axis.

by the symmetry of the cluster.[54] The single-crystal measurements made possible by the high symmetry of compound **3** provide invaluable information in further characterizing the magnetic properties of this decanuclear system. We attribute the magnetic anisotropy evident in the single-crystal susceptibility data for **3** to weak, axial zero-field splitting (D) of the high-spin $S = 12$ ground state for this cluster. This zero-field splitting (zfs) of the ground state probably arises from the single-ion anisotropy of the d^4 Mn(III) ions, as suggested by theoretical calculations (vide infra). This Ising-type anisotropy, with a unique easy axis, *c*, and a hard plane, indicates that the sign of the axial zfs parameter D should be negative with the $M_s = \pm 12$ doublet lowest in energy.

The single-crystal EPR data for **3** provide a spectacular demonstration of zero-field splitting of the high-spin $S = 12$ ground state and allow for a quantitative estimate of D, the axial zfs parameter. We assign the nine-line signal observed for **3** at 4 K, shown in Figure 6, to transitions within the $S = 12$ ground state multiplet. The fine structure of the spectrum, visible at fields above 5000 G, corresponds to the transitions $-3 \rightarrow -4$, $-4 \rightarrow -5$, up to $-11 \rightarrow -12$. In the range 0−5300 G, the spectrum is complicated not only by the presence of a broad signal at $g = 2.0$, probably arising from the isolated Mn(II) cation, but also by additional transitions of the type $-12 \rightarrow -11$, $-11 \rightarrow -10$, down to $-5 \rightarrow -4$. The separation between the lines depends on the magnitude of the zero-field splitting of the ground state. A spacing of 750 G is equal to $|2D|$, resulting in a value for $|D|$ of $|0.035|$ cm^{-1}. The sign of the zfs parameter is not provided by the EPR spectra but can be deduced by the single-crystal magnetic measurements as mentioned above.

By using the estimate of the zfs parameter D obtained from the EPR data, we were able to simulate the single-crystal magnetization curve for **3**. A simulated curve of reduced magnetization versus field for an $S = 12$ system with $D = -0.035$ cm^{-1}, and the field either parallel or perpendicular to the unique axis is shown together with the data in Figure 5. Given the complexity of such a high-spin system and the relative crudeness of this model, the agreement between the calculated and experimental values is excellent.

Very slow relaxation of the magnetization of a dodecanuclear manganese complex was recently published elsewhere,[29] opening new perspectives for magnetic memory at the molecular level. This complex has the formula $[Mn_{12}O_{12}(O_2CR)_{16}(H_2O)_4]$ (R = Ph, CH_3) and exhibits unprecedented relaxation phenomena through the combination of a high-spin ground state, $S = 10$, and a large Ising-type anisotropy. Such behavior suggests that our Mn_{10} system would be a good candidate for displaying similar superparamagnetic-like properties. Quantitative analysis of the magnetization curves shown in Figure 5 allowed for an estimation of the macroscopic anisotropy constant, K_1, which, to a first approximation, is given by the difference in the work required to saturate the magnetization parallel and perpendicular to the easy axis.[55] This constant was estimated to be 3.4×10^5 erg/cm^3, approximately 10 times smaller than K_1 for the Mn_{12} complex.[56] The relative size of K_1 is in close agreement with the magnitude expected if we compare the molecular anisotropy of the two compounds, given approximately by DS^2, which is about 5.0 cm^{-1} for **3** and 50 cm^{-1} for the Mn_{12} complex. The smaller number of Mn(III) centers in **3** is probably the reason for this large difference, even though structural parameters also play a role (vide infra).

The magnetization relaxation process follows an exponential law typical of a thermally activated process, having the form $\tau = \tau_0 \exp(\Delta/kBT)$, where τ_0 is the relaxation time at infinite temperature and Δ is proportional to K_1. These calculations show that compound **3** should have a much faster relaxation than the dodecanuclear complex, but superparamagnetic-like behavior should still be observable at temperatures not far below 1 K.[57]

In order to provide a theoretical basis for the observed magnetic properties of compounds **1**−**3**, and especially to offer a rationale for the high-spin ground state, we propose three related models for the exchange interactions in the Mn_{10} cluster, each one of increasing complexity. A schematic view of the spin topology of the cluster is given in Figure 7. The two $S = {}^5/_2$ and four $S = 2$ spins, which correspond to the Mn(II) atoms Mn(1) and Mn(8) and the Mn(III) atoms Mn(5), Mn(2), Mn(3), and Mn(10) in compounds **1** and **2**, are arranged at the vertices of an "inner core" octahedron. Four $S = {}^5/_2$ spins, corresponding to Mn(6), Mn(4), Mn(7), and Mn(9), cap the four faces of this octahedron, and we refer to these atoms as the "outer" Mn(II) atoms.

Only four distinct magnetic exchange pathways are assumed to be present. This assumption must be true for **3**, given the crystallographically-imposed D_{2d} symmetry, and is quite reasonable for the isostructural compounds **1** and **2**. The parameter J_{III} represents the coupling constant between Mn(III) atoms, the coupling between Mn(II) atoms is represented by J_{II}, the exchange between the Mn(III) and inner core Mn(II) atoms is labeled with J_c, and J_o represents the coupling between the

(54) Matrices ranging in dimension from 1 (for $S = 23$) to 266 360 (for $S = 5$) have to be diagonalized for a full-matrix calculation. The symmetry factorization reduces the dimension of the matrices by a factor of 4.

(55) Morrish, A. H. *The Physical Principles of Magnetism*; John Wiley and Sons: New York, 1966.

(56) By expressing the volume magnetization in emu/cm^3 and the magnetic field in Oe, the anisotropy constant has the dimensions of energy per volume unit, which is erg/cm^3 in cgs units.

(57) At such low temperatures, intercluster interactions may cause three-dimensional magnetic ordering in the solid state for **3.** Assuming that only through-space dipolar exchange is significant, one can calculate the dipolar energy, E_{dip}, associated with intercluster interactions, which allows for an estimation of the expected critical ordering temperature, T_c. A simple calculation was made for E_{dip} by placing a magnetic moment of 24 μ_B on the centroid of the cluster and one of 5 μ_B on the isolated Mn(II) cation. Interactions between all magnetic moments within a sphere of 80 Å were considered. The largest E_{dip} was ≈ 0.4 K, calculated for an antiferromagnetic structure with the magnetic cell double along *c*. The low value of T_c, which arises from the large separation between the complex anions, suggests that intercluster interactions will not preclude the observation of superparamagnetic relaxation effects for the Mn_{10} complex, and experiments are in progress to observe such behavior.

(58) Kambé, K. *J. Phys. Soc. Jpn.* **1950**, *5*, 48−51.

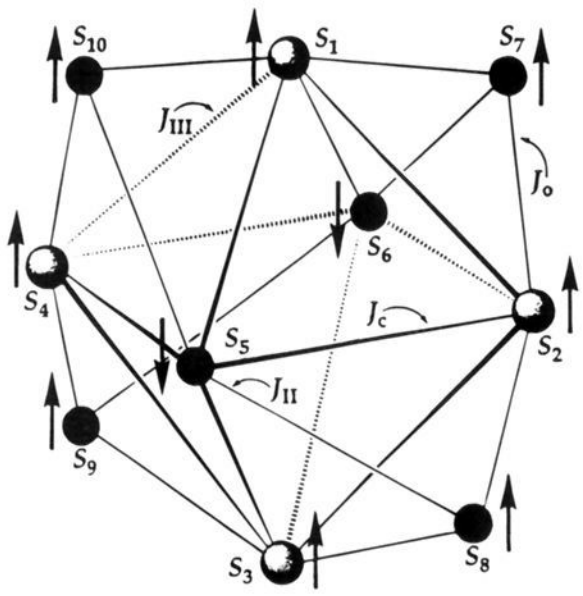

$S_1 \rightarrow Mn_2$ $S_6 \rightarrow Mn_8$
$S_2 \rightarrow Mn_5$ $S_7 \rightarrow Mn_6$
$S_3 \rightarrow Mn_{10}$ $S_8 \rightarrow Mn_9$
$S_4 \rightarrow Mn_3$ $S_9 \rightarrow Mn_7$
$S_5 \rightarrow Mn_1$ $S_{10} \rightarrow Mn_4$

Figure 7. Diagram of the spin topology and magnetic exchange coupling pathways for the $[Mn_{10}O_4(biphen)_4X_{12}]^{4-}$ anion ($X = Cl^-$, Br^-). Black spheres are Mn(II) sites, and gray spheres are Mn(III) sites. The large arrows represent the direction for the spin vectors at each manganese site as described by case a (see text). The relationship between the spin labels and the manganese atom labeling scheme of Figure 1 is also depicted.

Mn(III) and outer Mn(II) atoms. The μ_4-oxo bridges are assumed to be the dominant pathway of magnetic exchange coupling between Mn atoms. Although the μ_3-halide and μ_2-halide ligands could theoretically mediate the coupling, the fact that the magnetic data are extremely similar for **1** and **2** supports the assumption that the μ_4-oxo bridges dominate.

The three models of the exchange coupling put forth below assume Heisenberg exchange between all spins and have made no allowance for the single-ion anisotropy of the Mn(III) atoms. The first and most simple model takes into account only six spins, the four Mn(III) spins ($S = 2$) and the two Mn(II) spins ($S = {}^5/_2$) of the inner octahedral core, and only two independent exchange parameters, J_{III} and J_c. The spin Hamiltonian for this model is given in eq 2. An analytical expression for the

$$\mathscr{H}_1 = J_c[\mathbf{S}_1\cdot\mathbf{S}_5 + \mathbf{S}_1\cdot\mathbf{S}_6 + \mathbf{S}_2\cdot\mathbf{S}_5 + \mathbf{S}_2\cdot\mathbf{S}_6 + \mathbf{S}_3\cdot\mathbf{S}_5 + \mathbf{S}_3\cdot\mathbf{S}_6 + \mathbf{S}_4\cdot\mathbf{S}_5 + \mathbf{S}_4\cdot\mathbf{S}_6] + J_{III}[\mathbf{S}_1\cdot\mathbf{S}_2 + \mathbf{S}_1\cdot\mathbf{S}_4 + \mathbf{S}_2\cdot\mathbf{S}_3 + \mathbf{S}_3\cdot\mathbf{S}_4] \quad (2)$$

eigenvalues of the Hamiltonian in eq 2 was derived by using the Kambé operator replacement method[58] and is given in eq 3, where $\mathbf{S}_A = \mathbf{S}_1 + \mathbf{S}_3$, $\mathbf{S}_B = \mathbf{S}_2 + \mathbf{S}_4$, $\mathbf{S}_C = \mathbf{S}_5 + \mathbf{S}_6$, $\mathbf{S}_D = \mathbf{S}_A + \mathbf{S}_B$, and the total S value is $\mathbf{S}_{tot} = \mathbf{S}_C + \mathbf{S}_D$.

$$E(|\mathbf{S}_A,\mathbf{S}_B,\mathbf{S}_C,\mathbf{S}_D,\mathbf{S}_{tot}\rangle) = J_c[\mathbf{S}_{tot}(\mathbf{S}_{tot}+1) - \mathbf{S}_D(\mathbf{S}_D+1) - \mathbf{S}_C(\mathbf{S}_C+1)] + J_{III}[\mathbf{S}_D(\mathbf{S}_D+1) - \mathbf{S}_A(\mathbf{S}_A+1) - \mathbf{S}_B(\mathbf{S}_B+1)] \quad (3)$$

By using eq 3, values for the relative energies of the possible spin states were calculated as a function of the ratio of the coupling constants. Two sets of antiferromagnetic exchange coupling parameters, referred to as case a and case b below, were found which give rise to a high-spin ground state for the whole cluster. In the following discussion, we refer to two or more spins, the vector sum of which has the maximum possible value, as being parallel to one another. Although strictly speaking this designation is incorrect, it greatly simplifies the discussion.

Case a. If the ratio of $J_{III}/J_c \leq 0.5$, allowing for the possibility of ferromagnetic values for J_{III}, the model given by eqs 2 and 3 yields the ground state $|\mathbf{S}_A,\mathbf{S}_B,\mathbf{S}_C,\mathbf{S}_D,\mathbf{S}_{tot}\rangle = |4,4,5,8,3\rangle$. In this state the four $S = 2$ spins are aligned parallel to each other as denoted by $\mathbf{S}_D = 8$. The two $S = {}^5/_2$ spins are also parallel to each other because $\mathbf{S}_C = 5$ but must be antiparallel to the $S = 2$ spins to give $\mathbf{S}_{tot} = 3 = |\mathbf{S}_C - \mathbf{S}_D|$. Now let us consider the outer Mn(II) atoms: if the ratio $J_{II} > J_o$ holds, then the four outer $S = {}^5/_2$ spins would be aligned parallel to the $S = 2$ spins of the Mn(III) atoms, resulting in an $\mathbf{S}_{tot} = [(4 \times {}^5/_2) + 3] = 13$ ground state for the entire cluster.

Case b. If the ratio $3 \leq J_{III}/J_c \leq 5$ holds, then by using eq 3 the ground state is calculated to be $|4,4,5,1,4\rangle$. Given the definitions of $\mathbf{S}_A$, $\mathbf{S}_B$, and $\mathbf{S}_D$ above, this ground state must have $\mathbf{S}_1$ and $\mathbf{S}_3$ parallel to each other as well as $\mathbf{S}_2$ and $\mathbf{S}_4$ parallel to each other, but $\mathbf{S}_1$ and $\mathbf{S}_3$ are not parallel to $\mathbf{S}_2$ and $\mathbf{S}_4$. These pairs of $S = 2$ spins must be oriented at some angle such that the resultant spin is $\mathbf{S}_D = 1.0$. A total spin of $\mathbf{S}_{tot} = 4 = |\mathbf{S}_C - \mathbf{S}_D|$ for the inner core is thus obtained. Again, we now consider the outer $S = {}^5/_2$ spins. If $J_o > J_{II}$, then the four outer $S = {}^5/_2$ spins will be aligned antiparallel to the vectorial sum $\mathbf{S}_D$ but parallel to the two inner core Mn(II) spins. This configuration results in a total spin for the cluster given by $\mathbf{S}_{tot} = [(4 \times {}^5/_2) - 1 + (2 \times {}^5/_2)] = 14$.

In order to substantiate either case a or case b as the configuration most likely to be responsible for the high-spin ground state of the Mn_{10} complex, the spin Hamiltonian shown in eq 4 was used, which is an expansion of eq 2. This second

$$\mathscr{H}_2 = \mathscr{H}_1 + J_o[\mathbf{S}_1\cdot\mathbf{S}_7 + \mathbf{S}_2\cdot\mathbf{S}_7] + J_{II}\mathbf{S}_6\cdot\mathbf{S}_7 \quad (4)$$

model includes seven manganese ions, six of the inner core plus one outer Mn(II) ion labeled S_7 in Figure 7. The eigenvalues for the possible spin states were obtained in numerical form from a full-matrix diagonalization of the Hamiltonian in eq 4.[59] The ratios between J_o and J_{II} necessary to obtain high-spin ground states for case a and case b were investigated. For case a, in which the initial condition is $J_{III}/J_c \leq 0.5$, a high-spin ground state of $S = 11/2$, which corresponds to $\mathbf{S}_{tot} = 13$ for the whole cluster, is found when the ratio $J_{II}/J_o > 2$ is satisfied. For case b, in which the initial condition is $3 \leq J_{III}/J_c \leq 5$, a ground state of $S = 13/2$, which corresponds to $\mathbf{S}_{tot} = 14$ for the entire cluster, is not obtained for any ratio of coupling parameters. The highest spin ground state attainable for case b is $S = 11/2$, in which the two conditions $J_c > J_{II}$ and $J_c > J_o$ have to be met. The failure of case b to yield an $\mathbf{S}_{tot} = 14$ ground state suggests that "arrows-up arrows-down" arguments for predicting the magnetic behavior of such a complex system is inappropriate, especially when conflicting antiferromagnetic interactions are present.

The third and most complex model incorporated four $S = 1$ and six $S = {}^3/_2$ spins in place of the actual $S = 2$ and $S = {}^5/_2$ spins of the real cluster. The spin Hamiltonian for this model is shown in eq 5, again an extension of eq 2. As in the second

$$\mathscr{H}_3 = \mathscr{H}_1 + J_o[\mathbf{S}_1\cdot\mathbf{S}_7 + \mathbf{S}_1\cdot\mathbf{S}_{10} + \mathbf{S}_2\cdot\mathbf{S}_7 + \mathbf{S}_2\cdot\mathbf{S}_8 + \mathbf{S}_3\cdot\mathbf{S}_8 + \mathbf{S}_3\cdot\mathbf{S}_9 + \mathbf{S}_4\cdot\mathbf{S}_9 + \mathbf{S}_4\cdot\mathbf{S}_{10}] + J_{II}[\mathbf{S}_6\cdot\mathbf{S}_7 + \mathbf{S}_5\cdot\mathbf{S}_8 + \mathbf{S}_6\cdot\mathbf{S}_9 + \mathbf{S}_5\cdot\mathbf{S}_{10}] \quad (5)$$

(59) The locally-written program CLUMAG was used, which takes advantage of the irreducible tensor operators method. See also: Gatteschi, D.; Pardi, L. *Gazz. Chim. Ital.* **1993**, *123*, 231−240.

Table 4. Total Spin, S_{tot}, of the Ground State for Case a as a Function of the Exchange Coupling Constants, with $J_{III} = -5$ cm^{-1} and $J_o = 10$ cm^{-1} [a]

	J_{II}							
J_c	1	2.5	5	10	20	30	40	50
10	5	5	5	3	1	1	1	1
20	5	5	5	4, 5, 3[b]	5	7	7	7
30	5	5	5	6, 7[b]	7	7	7	7
40	5	5	5	5	7	7	7	7
50	5	5	5	5	7	7	7	7

[a] Values for J_{II} and J_c given in cm^{-1}. [b] Multiple entries indicate that the model calculations gave two or more spin states close in energy to the ground state.

Table 5. Total Spin, S_{tot}, of the Ground State for Case b as a Function of the Exchange Coupling Constants, with $J_c = 5$ cm^{-1} and $J_{III} = 20$ cm^{-1} [a]

	J_o						
J_{II}	6	8	10	12	14	16	18
0	8	7	7	7	6	6	6
1	0, 1, 2, 3	7	7	7	6	6	6
2	0, 1, 2, 3	0, 1, 2, 3	0, 1, 2, 3	7, 6, 6, ...	6	6	6
3	0, 1, 2, 3	0, 1, 2, 3	0, 1, 2, 3	4, 3	5, 6, 4, ...	6	6
4	0, 1, 2, 3	0, 1, 2, 3	0, 1, 2, 3	4, 3	4, 5, 4, ...	5, ..., 1	4, ..., 0
5	0, 1, 2, 3	0, 1, 2, 3	0, 1, 2, 3	4	4	5, 4	5, 4

[a] Values for J_o and J_{II} given in cm^{-1}.

model, numerical calculations of the eigenvalues of the possible spin states were performed through full-matrix diagonalization of eq 4.[59,60] Again, cases a and b were investigated to find which ratios of the exchange parameters resulted in high-spin ground states or reproduced other experimental observations.

Ground states obtained from a series of calculations for case a are shown in Table 4. In these calculations two of the coupling constants, J_c and J_{II}, were varied, while J_o and J_{III} were fixed at 10 and -5 cm^{-1}, respectively. In this model, a spin ground state of $S = 7$ corresponds to both $S = 12$ and $S = 13$ for the actual cluster, since there is not a one-to-one correspondence between the states of the reduced and the actual system given the many more possible S states for the latter. As shown in Table 4, in addition to the requirement of $J_{III}/J_c < 0.5$ for case a, J_c and J_{II} must be two times larger than J_o to produce a high-spin ground state.

Fixing $J_c = 5$ cm^{-1} and $J_{III} = 20$ cm^{-1}, which satisfies the requirement for case b, and allowing J_{II} and J_o to vary led to the results shown in Table 5. In this case, high-spin ground states are observed for only a small region of the parameter space, and for most of them, the energy levels are very closely spaced. Several calculations showed 100 states to lie within 10 cm^{-1} of the ground state.

Although these models only yield qualitative results about the nature of the ground spin state, we can conclude that the large-spin ground states for **1**–**3** can be found in two well-separated regions of parameter space defined by the following relations: (case a) $J_{III} < J_o < J_c \approx J_{II}$ and (case b) $J_{II} < J_c < J_o < J_{III}$. We suggest that case a is in fact the correct description for the spin topology of the ground states for compounds **1**–**3**. Several examples are available of complexes that exhibit very weak antiferromagnetic or even weak ferromagnetic coupling between Mn(III) centers mediated by μ-oxo bridging ligands. In these examples the Mn–O–Mn angles are close to 120°, as in **1**–**3**.[61] Antiferromagnetic coupling between Mn(II) and Mn(III) sites through oxo bridges appears to increase with an increase of the M–O–M angle from 100° to 115°, supporting the condition $J_c > J_o$, as is found for case a.[13]

(60) The D_{2d} point group symmetry of the Mn_{10} cluster was used to reduce the dimensions of the matrices before diagonalization.

(61) See Table VI in ref 13.

Several pieces of experimental evidence favor case a as being the correct description. The high-field magnetization data for compounds **1** and **2** exhibit a smooth plateau, implying that the ground state is well-separated at high field. Compound **3** clearly exhibits a well-separated $S = 12$ ground state from the rounded maximum observed for the polycrystalline susceptibility data. All of these data are incompatible with the results found for case b, in which several excited spin states lie close in energy to the high-spin ground state. The results of the model calculations showed that, in case a, the spin of the ground state is much less sensitive to the exact values of the exchange coupling constants compared to that of case b. The fact that large-spin ground states are observed in all three complexes **1**, **2**, and **3** suggests that model a is a better representation of the exchange interactions than model b. Case a predicts an $S = 13$ ground state, and the high-field magnetization data for **2** show a plateau value close to that expected for $S = 14$. The calculations for the reduced spin system of model 3 show that the $S = 14$ state should not lie close in energy to the $S = 13$ state, but the extension from the reduced model to the real system is not straightforward.

If a ground state of $S = 13$ arises from the coupling scheme of case a, the zero-field splitting of the fully coupled $S = 13$ state can be easily correlated in the strong exchange limit to the single-ion zero-field splitting of the individual Mn ions in the cluster.[62] Assuming the zero-field splitting to be dominated by the Jahn–Teller distorted Mn(III) atoms, the D value obtained from the EPR data, $D_{(S=13)} = -0.035$ cm^{-1}, corresponds to $D_{Mn(III)} = -1.94$ cm^{-1}. This value agrees with data in the literature,[63] although it is lower than that found for the Mn_{12} system previously described. The difference probably arises from the greater non-collinearity of the elongated Jahn–Teller Mn(III) axes in compounds **1**–**3** compared to that in the Mn_{12} compound. The $S = 12$ ground state observed for **3** must come from a configuration very close to that described by case a, and a similar relation of the zfs parameters holds. We favor case a as the most reasonable description of the exchange interactions and spin orientation for the Mn_{10} complex. Experimental proof of the spin orientation and correct set of exchange constants may only come from obtaining a spin density map from a single-crystal polarized neutron diffraction study.[64]

Conclusions

We have synthesized and structurally characterized novel decanuclear mixed-valent manganese complexes. A detailed examination of the rich magnetic properties of these cluster anions has been successfully carried out, confirming their remarkably high-spin ground states. Substitution of Br^- for Cl^- has little effect on the overall magnetic properties of this system. Single-crystal magnetic measurements have allowed for characterization of the spin ground state, including a quantitative analysis of the Ising-type anisotropy manifest in the susceptibility and magnetization measurements. The zfs parameter, D, was estimated from single-crystal EPR data and successfully used to simulate the magnetization data. Several theoretical approaches were employed to explain the high-spin ground state and describe the exchange interactions of this high-nuclearity cluster, and a plausible hypothesis consistent with all of the data was developed. The synthesis and magnetic characteriza-

(62) Bencini, A.; Gatteschi, D. *EPR of Exchange Coupled Systems*; Springer Verlag: Berlin, 1990.

(63) Kennedy, B. J.; Murray, K. S. *Inorg. Chem.* **1985**, *24*, 1552–1557.

(64) **Note Added in Proof:** High-frequency (245 GHz) EPR spectra recorded on a polycrystalline sample of **1** strongly suggest that the ground state for this compound has $S = 12$ with negative zero-field splitting, as suggested for **3**. HF-EPR data on **2** are not yet available.

tion of such systems has far-reaching applications for understanding high-spin polynuclear clusters found in biological systems, as well as in the development of new kinds of magnetic molecular materials.

Acknowledgment. We thank E. McNiff, Jr., of the Francis Bitter National Magnet Laboratory for assistance in obtaining the high-field magnetization data and Dr. S. Herold for useful discussions. This work was supported by a grant from the NSF (to S.J.L.). Prof. D. Gatteschi and Dr. L. Pardi kindly provided the CLUMAG program used to calculate the energies of the spin levels. A.C. acknowledges the Consiglio Nazionale delle Ricerche, Comitato Nazionale Scienze Chimiche, for support of his stay at MIT.

Supplementary Material Available: Tables of complete atomic positional parameters and B_{eq}, intramolecular bond distances and angles, and anisotropic thermal parameters for **2** (24 pages). This material is contained in many libraries on microfiche, immediately follows this article in the microfilm version of the journal, can be ordered from the ACS, and can be downloaded from the Internet; see any current masthead page for ordering information and Internet access instructions.

JA944124L